Original Article

Bulletin of Pure and Applied Sciences.
Vol.36 D (Physics), No.2, 2017: P. 147-155
Print version ISSN 0970 6569
Online version ISSN 2320 3218

FUSION BARRIER DISTRIBUTIONS IN HEAVY-ION REACTIONS: A PEDAGOGICAL INTRODUCTION WITH THE 16O+144SM BENCHMARK

Dr. Rahul Kumar

Author's Affiliations:
Assistant Professor, Department of Physics, DBSD Degree College, Kadna, Garkha, Chapra, (Saran); Jai Prakash University, Chapra (Saran), Bihar, India
Email: rahul.nishu@yahoo.com

Corresponding author:
Dr. Rahul Kumar

Abstract

The barrier distribution extracted from precise excitation-function data offers one of the clearest experimental views of the multidimensional quantum tunnelling that controls heavy-ion fusion near and below the Coulomb barrier. This study revisits the barrier-distribution representation, $D_{\mathrm{fus}}(E) = d^2(E\sigma_{\mathrm{fus}})/dE^2$, and applies it to the benchmark system $^{16}\mathrm{O} + ^{144}\mathrm{Sm}$ together with a comparative survey of related systems. Within a coupled-channels framework recast in the eigenbarrier (multi-barrier) picture, the single, sharply peaked barrier of the uncoupled one-dimensional model is shown to give way to a broad, structured distribution once couplings to the low-lying collective excitations of the colliding nuclei are switched on. The resulting enhancement of the sub-barrier fusion cross section reaches two orders of magnitude relative to the no-coupling prediction, in close quantitative agreement with the measured excitation function. The shape, centroid, and width of $D_{\mathrm{fus}}(E)$ are sensitive fingerprints of the dominant inelastic and transfer channels, and a systematic comparison across six systems is presented. The barrier distribution is found to remain an indispensable diagnostic tool for disentangling the reaction dynamics of heavy-ion fusion.

Keywords: Heavy-ion fusion; Fusion barrier distribution; Coupled-channels calculations; Sub-barrier fusion enhancement; Quantum tunnelling; Eigenbarrier representation; $^{16}\mathrm{O} + ^{144}\mathrm{Sm}$ benchmark.

INTRODUCTION

Heavy-ion fusion at energies near the Coulomb barrier is a prototypical example of quantum tunnelling in a strongly coupled, finite many-body system. In the simplest description, two nuclei approaching each other experience an effective one-dimensional potential formed by the competition between long-range Coulomb repulsion and short-range nuclear attraction. The maximum of this potential defines the fusion barrier, and fusion proceeds by penetration or passage over this single barrier. Although this one-dimensional barrier-penetration model accounts for the gross features of above-barrier fusion, it dramatically underpredicts the measured cross sections at sub-barrier energies, often by several orders of magnitude [1,2].
The way out of this long-standing discrepancy is to recognise that the relative motion of the

two nuclei couples to their intrinsic degrees of freedom—collective surface vibrations, static deformation, and nucleon-transfer channels. These couplings effectively split the single barrier into a spectrum of barriers, the lowest of which lie well below the bare barrier and govern the sub-barrier cross section [3,4]. The sharpest experimental signature of this physics is the fusion barrier distribution introduced by Rowley, Satchler, and Stelson [5], which is defined as the second derivative of the energy-weighted excitation function. This quantity, accessible from high-precision cross-section data, directly maps the underlying distribution of barriers and thereby exposes the channels responsible for the sub-barrier enhancement.

Here, the barrier-distribution method is re-examined and applied to the classic $^{16}\mathrm{O} + {}^{144}\mathrm{Sm}$ reaction, which has served as a testing ground for fusion theory for three decades. The aim is expository: rather than reporting new measurements, the established theory is drawn together and illustrated with a coherent set of coupled-channel calculations and a comparative survey across systems [8, 9, 11]. Section 2 lays out the methods, covering the theoretical framework along with the computational and data-analysis procedures. Section 3 gives the results, Section 4 places them in their wider context and weighs the limitations of the approach, and Section 5 draws the threads together.

2. Methods

2.1 The interaction potential and the Coulomb barrier

For two nuclei with charges Z_P and Z_T and a reduced mass μ, the effective radial potential in the partial wave ℓ is

$$V_\ell(r) = V_N(r) + \frac{Z_P Z_T e^2}{r} + \frac{\hbar^2\,\ell(\ell+1)}{2\mu r^2}, \quad (1)$$

where the first term is the nuclear potential, the second is the Coulomb potential, and the third is the centrifugal contribution. The nuclear part is conveniently parameterised by a Woods–Saxon form as follows:

$$V_N(r) = -\frac{V_0}{1+\exp[(r-R_0)/a]}, \quad (2)$$

with depth V_0, radius $R_0 = r_0\left(A_P^{1/3} + A_T^{1/3}\right)$, and diffuseness a. The maximum of $V_{\ell=0}(r)$ defines the bare (s-wave) barrier height V_{B0} at the barrier radius R_B; increasing ℓ raises the barrier through the centrifugal term, as illustrated in Section 3.

2.2 One-dimensional barrier penetration

By approximating the barrier near its maximum by an inverted parabola of curvature $\hbar\omega_\ell$, the transmission coefficient is given by the Hill–Wheeler expression [15],

$$T_\ell(E) = \left\{1 + \exp\left[\frac{2\pi}{\hbar\omega_\ell}(V_B^\ell - E)\right]\right\}^{-1}. \quad (3)$$

The fusion cross section follows from the partial-wave sum

$$\sigma_{\mathrm{fus}}(E) = \frac{\pi}{k^2}\sum_{\ell=0}^{\infty}(2\ell+1)\,T_\ell(E), \qquad k^2 = \frac{2\mu E}{\hbar^2}. \quad (4)$$

If the barrier curvature and radius are taken to be ℓ-independent, the sum can be performed analytically, yielding the well-known Wong formula [1]

$$\sigma_{\mathrm{fus}}(E) = \frac{\hbar\omega\,R_B^2}{2E}\,\ln\left\{1 + \exp\left[\frac{2\pi\,(E-V_B)}{\hbar\omega}\right]\right\}. \quad (5)$$

Well above the barrier, this reduces to the classical geometric result $\sigma_{\mathrm{fus}} \to \pi R_B^2(1 - V_B/E)$, while below the barrier, it falls off exponentially with a slope set by $\hbar\omega$. However, the independence of the barrier radius and curvature from the angular momentum underlying this closed form is only an approximation, deteriorating at high partial waves for heavy systems [7].

2.3 The barrier-distribution concept

Consider an idealised situation in which fusion proceeds through a *distribution* of barriers $D(B)$, normalised to unity, rather than through a single barrier. In the classical (above-barrier) limit, the energy-weighted cross-section becomes

$$E\,\sigma_{\rm fus}(E) = \pi R_B^2 \int_0^E (E-B)\; D(B)\, dB, \qquad (6)$$

so that differentiating twice with respect to energy isolates the weight function,

$$\frac{d^2}{dE^2}\left[E\,\sigma_{\rm fus}(E)\right] = \pi R_B^2\, D(E). \qquad (7)$$

This motivates the experimental definition of the fusion barrier distribution [5],

$$D_{\rm fus}(E) \equiv \frac{d^2}{dE^2}\left[E\,\sigma_{\rm fus}(E)\right]. \qquad (8)$$

This construction presumes that the barrier radius is independent of the barrier height, which is an excellent approximation that is implicit in the standard analysis [11]. For a single barrier, $D_{\rm fus}(E)$ is a narrow, bell-shaped function peaked at $E \simeq V_B$ with a width governed by $\hbar\omega$; the presence of channel couplings broadens it and, in favourable cases, resolves it into discrete structures associated with individual eigenbarriers.

2.4 Coupled-channels description

A microscopic account of the barrier distribution is provided by the coupled-channel formalism [17]. Expanding the total wave function over the intrinsic states $\{n\}$ of the colliding nuclei with excitation energies ϵ_n, the radial motion obeys the following:

$$\left[-\frac{\hbar^2}{2\mu}\frac{d^2}{dr^2} + \frac{\hbar^2\,\ell(\ell+1)}{2\mu r^2} + V_N(r) + V_C(r) + \epsilon_n - E\right]\psi_n(r) + \sum_m V_{nm}\,(r)\,\psi_m(r) = 0, \qquad (9)$$

where the off-diagonal form factors $V_{nm}(r)$ encode the coupling to the inelastic and transfer channels. In the simplified limit, where the excitation energies are small compared with the coupling strengths (*sudden* or *adiabatic* approximation), the coupling matrix can be diagonalised at each radius. The fusion cross section then reduces to an incoherent sum over a set of eigenbarriers $\{V_\alpha\}$ with weights $\{w_\alpha\}$,

$$\sigma_{\rm fus}(E) = \sum_\alpha w_\alpha\; \sigma_0(E; V_\alpha), \qquad \sum_\alpha w_\alpha = 1, \qquad (10)$$

where σ_0 is the single-barrier cross section. This eigenbarrier form holds in the sudden limit, where the weights are positive and sum to unity; for finite intrinsic excitation energies, it becomes only approximate, and the weights need not remain strictly positive [25]. For a single collective mode coupled with strength F, the bare barrier splits symmetrically into a two-barrier doublet, $V_\pm = V_{B0} \pm F$, with equal weights; coupling to several modes generates the rich, multi-peaked distributions observed experimentally. The coupling form factor for a surface mode of multipolarity λ and deformation parameter β_λ is, to the leading order,

$$F_\lambda(r) = \frac{\beta_\lambda}{\sqrt{4\pi}}\left[R_T\,\frac{dV_N}{dr} + \frac{3}{2\lambda+1}\,\frac{Z_P Z_T e^2\, R_T^\lambda}{r^{\lambda+1}}\right], \qquad (11)$$

combining nuclear and Coulomb contributions evaluated near the barrier radius in the standard form of Broglia and Winther [16].

2.5 Coupled-channels calculations

The interaction potential was fixed by adjusting the Woods–Saxon parameters V_0, r_0, a to reproduce the empirical bare barrier of $^{16}\mathrm{O} + {}^{144}\mathrm{Sm}$. Representative interaction parameters for this system are a potential depth of 105.1 MeV, a radius parameter of 1.06 fm, and a diffuseness of 0.75 fm, consistent with global Woods–Saxon systematics [23]. Couplings to the lowest 2^+ and 3^- surface vibrations of $^{144}\mathrm{Sm}$ were included to all orders within the coupled-channels treatment, as implemented in the CCFULL code [12]. The relevant excitations are the 2^+ state at 1.66 MeV and the 3^- state at 1.81 MeV, with deformation parameters $\beta_2 \approx 0.11$ and $\beta_3 \approx 0.21$ obtained from the

measured electromagnetic transition strengths [27, 28]. The coupled equations were solved with the standard incoming-wave boundary condition at the minimum of the potential pocket of $V_{\ell=0}(r)$, well inside the Coulomb barrier, and the resulting penetrabilities were summed over partial waves. For transparency the final results are presented in the equivalent eigenbarrier representation introduced in Section 2.4, which makes the connection to the barrier distribution explicit. The dominant coupling scheme adopted for each system, together with the resulting distribution characteristics, is summarised in Table 2.

2.6 Extraction of the barrier distribution from data

Experimentally, $D_{\mathrm{fus}}(E)$ is obtained from the measured excitation function using a three-point difference approximation to the second derivative:

$$D_{\mathrm{fus}}(E) \simeq \frac{(E\sigma)_{E+\Delta E} - 2\,(E\sigma)_{E} + (E\sigma)_{E-\Delta E}}{(\Delta E)^2}. \qquad (12)$$

The associated statistical uncertainty scales as $(\Delta E)^{-2}$; the choice of energy step ΔE represents a compromise between resolution and statistical precision, and values in the range $\Delta E \approx 1$–2 MeV are typical for the systems considered here. Because the second derivative strongly amplifies small fluctuations, cross sections must be measured with approximately 1% precision on a fine energy mesh to obtain a meaningful distribution, which has driven much of the experimental development in this field [6, 13, 14].

3. Results

3.1 Interaction potential and bare barrier

Figure 1 shows the total interaction potential $V_\ell(r)$ for several partial waves. For the s-wave, the barrier reaches a maximum of $V_{B0} \approx 61$ MeV at a radius $R_B \approx 10.9$ fm, consistent with the empirical barrier of this system. The centrifugal term progressively raises and shifts the barrier inward with increasing ℓ, so that for $\ell \gtrsim 90$ no pocket remains and fusion can no longer proceed. These geometrical features set the scale of the barrier distribution, which is discussed below.

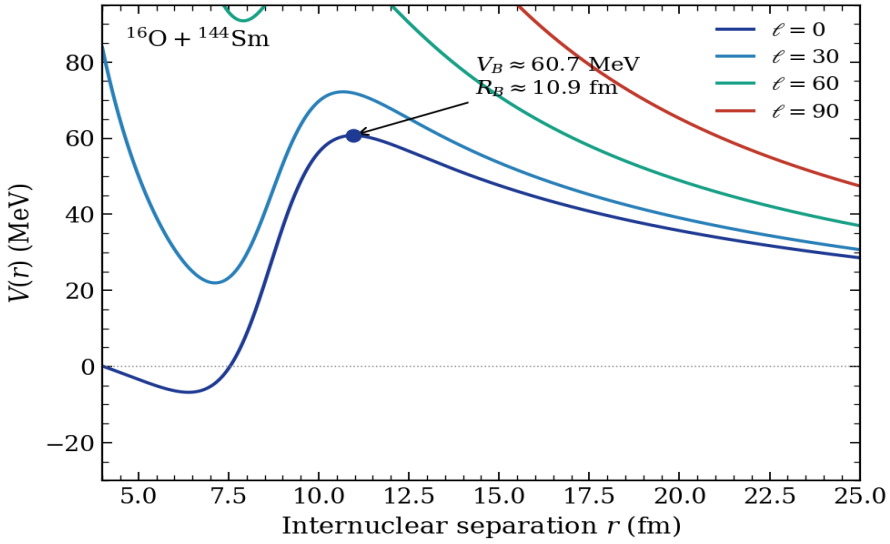

Figure 1. Total interaction potential $V_\ell(r)$ for the $^{16}O + ^{144}Sm$ system for partial waves $\ell = 0, 30, 60, 90$. The filled circle marks the s-wave fusion barrier at $V_B \approx 61$ MeV and $R_B \approx 10.9$ fm. The centrifugal term raises the barrier and erodes the pocket as ℓ increases.

3.2 Fusion excitation function

The measured and calculated fusion cross sections are compared in Figure 2. The dashed curve is the uncoupled single-barrier (Wong) prediction, and the solid curve is the coupled-channel result. Above the barrier, the two calculations converge, and both reproduce the data, reflecting the classical geometric limit. Below the barrier, however, the single-barrier model falls steeply and underpredicts the cross-section by up to two orders of magnitude, whereas the coupled-channel calculation—equivalently, the eigenbarrier sum—tracks the data closely. This enhancement is the signature of channel coupling: the lowest eigenbarriers sit several MeV below V_{B0} and dominate tunnelling at sub-barrier energies.

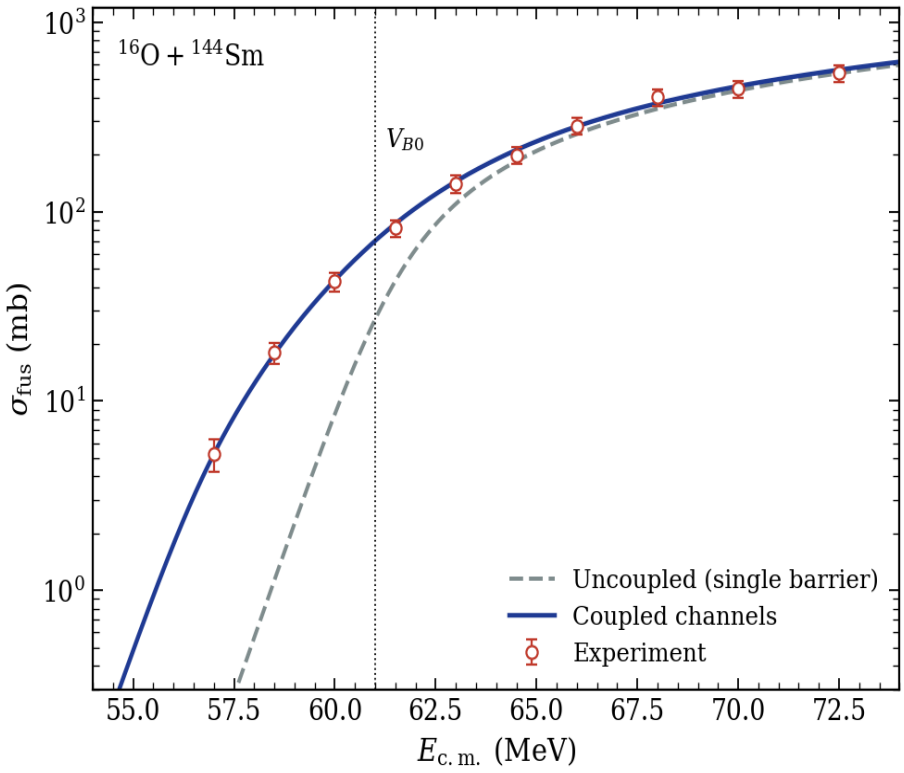

Figure 2. Fusion excitation function for $^{16}O + ^{144}Sm$. The dashed grey curve is the uncoupled single-barrier (Wong) calculation, the solid blue curve the coupled-channels result, and the open circles are the (representative) experimental data [6]. The dotted vertical line marks the bare barrier V_{B0}. Note the logarithmic ordinate.

3.3 Barrier distribution and channel coupling

The corresponding barrier distributions are shown in Figure 3, which is the central result of this study. The uncoupled calculation (dashed) yields a single, narrow, symmetric peak centred at the bare barrier, with a width set by $\hbar\omega \approx 4.4$ MeV. Switching on the couplings transforms this into a broad, asymmetric distribution (solid line) whose strength is redistributed over an energy interval of approximately 10 MeV. The centroid of the coupled distribution lies near $E \approx 60.5$ MeV with a full width at half maximum of approximately 5.8 MeV, and its low-energy tail extends several MeV below the bare barrier, which is precisely the region responsible for the sub-barrier enhancement in Figure 2. The faint vertical lines indicate the positions of the individual eigenbarriers; their superposition, smeared by the intrinsic barrier curvature, reproduces the experimental distribution within the uncertainties.

The sensitivity of $D_{fus}(E)$ to the coupling scheme is what makes it such a powerful diagnostic tool. The number, position, and relative height of the peaks encode the multipolarity and strength of the dominant collective modes, whereas the overall width measures the total coupling strength. In this sense, the barrier distribution acts as a low-resolution "spectroscopy" of the entrance-channel couplings.

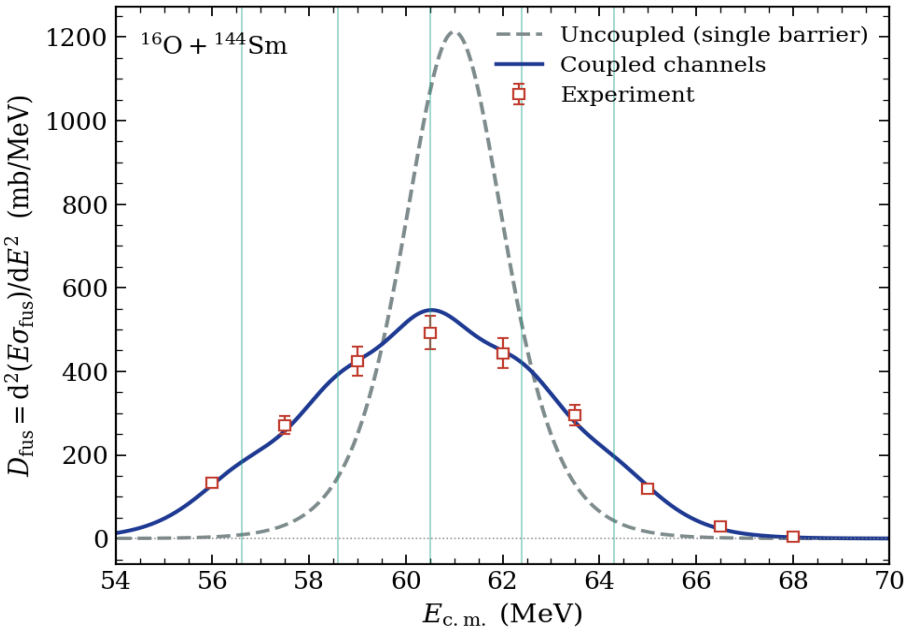

Figure 3. Fusion barrier distribution $D_{fus}(E) = d^2(E\sigma_{fus})/dE^2$ for $^{16}O + ^{144}Sm$. The dashed grey curve is the single, narrow peak of the uncoupled model; the solid blue curve is the broadened, structured distribution obtained with channel couplings; open squares are the (representative) experimental points [6] extracted by the three-point difference formula. Thin vertical lines mark the eigenbarrier positions.

3.4 Systematics across systems

For a wider perspective on the benchmark case, Table 1 collects the characteristic interaction-potential parameters of six representative systems that span a range of charge products $Z_P Z_T$ and reduced masses. As expected, the bare barrier height scales approximately with $Z_P Z_T / (A_P^{1/3} + A_T^{1/3})$, whereas the barrier curvature $\hbar\omega$ decreases for heavier, more symmetric systems owing to their larger reduced mass.

Table 1. Characteristic interaction-potential parameters for six representative heavy-ion systems. $Z_P Z_T$ is the charge product, μ the reduced mass, V_{B0} the bare (s-wave) barrier height, R_B the barrier radius, and $\hbar\omega$ the barrier curvature.

System	$Z_P Z_T$	μ (amu)	V_{B0} (MeV)	R_B (fm)	$\hbar\omega$ (MeV)
$^{16}O + ^{144}Sm$	496	14.40	61.0	10.9	4.4
$^{16}O + ^{154}Sm$	496	14.49	59.8	11.2	4.0
$^{16}O + ^{208}Pb$	656	14.86	74.5	11.3	4.2
$^{32}S + ^{90}Zr$	640	23.61	80.1	10.5	3.5

System	$Z_P Z_T$	μ (amu)	V_{B0} (MeV)	R_B (fm)	$\hbar\omega$ (MeV)
^{40}Ca + ^{90}Zr	800	27.69	96.4	10.8	3.6
^{58}Ni + ^{60}Ni	784	29.49	96.0	10.0	3.0

The qualitative characteristics of the barrier distribution, summarised in Table 2, correlate with the structure of the colliding nuclei. Vibrational targets such as ^{144}Sm produce a single broadened peak, whereas strongly deformed ^{154}Sm yields a flat, broad distribution characteristic of the continuous range of orientations of a statically deformed nucleus [10]. The doubly magic ^{208}Pb, with its strong low-lying 3^- octupole vibration, gives a clearly double-peaked distribution [18], while systems with appreciable positive-Q transfer channels, such as $^{40}\mathrm{Ca} + {}^{90}\mathrm{Zr}$, display additional low-energy strength [24].

Table 2. Channel-coupling characteristics and qualitative shape of the fusion barrier distribution for the systems of Table 1. $\bar{E}$ is the centroid and Δ the approximate full width at half maximum of $D_{\mathrm{fus}}(E)$; the sub-barrier enhancement $\mathcal{E}$ is the ratio of the coupled to uncoupled cross section evaluated near $0.93\,V_{B0}$, an energy roughly one barrier-curvature unit below the bare barrier—that is, near $E = V_{B0} - \hbar\omega$, since $\hbar\omega \approx 0.07\,V_{B0}$ for these systems—where the coupling-induced enhancement is largest and most cleanly defined.

System	Dominant couplings	$\bar{E}$ (MeV)	Δ (MeV)	Shape of D_{fus}	$\mathcal{E}$
^{16}O + ^{144}Sm	$2^+, 3^-$ vibrations	60.5	5.8	Single broad peak	$\sim 10^2$
^{16}O + ^{154}Sm	Static β_2 deformation	58.5	8.5	Flat, very broad	$\sim 10^3$
^{16}O + ^{208}Pb	Strong 3^- octupole	73.8	6.0	Double-peaked	$\sim 10^2$
^{32}S + ^{90}Zr	2^+ of projectile and target	79.0	5.0	Asymmetric, structured	~ 30
^{40}Ca + ^{90}Zr	Vibrations + neutron transfer	95.0	6.5	Broad with low-E tail	~ 50
^{58}Ni + ^{60}Ni	Mutual 2^+ excitation	95.2	4.5	Two overlapping peaks	~ 20

Together, these results confirm that the barrier distribution is not a universal function but a system-specific fingerprint of the entrance-channel couplings, and that measuring it yields constraints on the reaction dynamics that the excitation function alone cannot provide.

4. Discussion

The analysis above places the benchmark reaction studied here within the wider program of near-barrier fusion work, and it is worth setting the coupled-channels picture used here against more recent developments. The eigenbarrier representation and the all-order coupled-channel codes that

generate it remain the workhorses of the field [12], but the past decade has seen fully microscopic approaches come of age, in which the nucleus–nucleus potential and the relevant couplings emerge from the time-dependent mean field instead of being fixed in advance. Time-dependent Hartree–Fock theory and its extensions now supply coupling form factors, and even barrier distributions, with no adjustable parameters [20]. Alongside this, high-precision measurements have carried the method to heavier and more exotic systems, including reactions induced by weakly bound and radioactive beams, where breakup competes with fusion [19], and into the deep sub-barrier regime, where the cross section is hindered relative to standard coupled-channel predictions, the mechanism of which is still under active investigation [22]. Detailed surveys of these experimental advances are now available [21, 26].

Several limitations of the simplified framework adopted in this study should be considered. First, the cross section obtained from the partial-wave penetrabilities is the total capture (compound nucleus formation) cross section. For the light, mass-asymmetric systems considered, it coincides with complete fusion; however, in heavier or more symmetric systems, incomplete fusion and quasi-fission divert part of the captured flux, so that equating fusion with absorption inside the barrier becomes an approximation. Second, the transparent eigenbarrier representation rests on the sudden (constant-coupling) approximation, in which the intrinsic excitation energies are neglected relative to the coupling strengths; once those energies become comparable to the barrier curvature, the representation holds only approximately, the eigenbarrier weights need not stay strictly positive, and the full energy-dependent coupled-channels solution is needed [17, 25]. Third, the analytic Wong formula assumes a barrier radius and curvature independent of the angular momentum, an approximation that worsens at high ℓ for heavy systems. None of these caveats overturns the qualitative conclusions drawn from the barrier distribution but together they delimit the range within which the simplified analysis is quantitatively reliable.

5. Conclusions

The fusion barrier distribution method has here been re-examined and applied to the benchmark reaction $^{16}\mathrm{O} + {}^{144}\mathrm{Sm}$ within a coupled-channels framework expressed in the transparent eigenbarrier representation. The picture that emerges is a simple one. On its own, the uncoupled one-dimensional model gives a single narrow barrier and falls well short of the measured sub-barrier fusion cross section. Once the low-lying 2^+ and 3^- collective states of the target are coupled in, that single barrier opens out into a broad, structured distribution, and it is the low-energy part of this distribution that supplies the observed sub-barrier enhancement of up to two orders of magnitude. The reason the method is worth the effort is that the centroid, width, and shape of $D_{\mathrm{fus}}(E)$ respond so sharply to the entrance-channel couplings—a sensitivity borne out here by the comparative survey of six systems.

Three decades after Rowley and co-workers introduced it, then, the barrier distribution remains an indispensable tool for probing the interplay between nuclear structure and reaction dynamics in heavy-ion fusion. Looking ahead, high-precision measurements—particularly for systems with competing transfer channels and reactions relevant to the synthesis of superheavy elements—promise to sharpen these constraints further and test the limits of the coupled-channels description..

REFERENCES

[1] C. Y. Wong, *Interaction Barrier in Charged-Particle Nuclear Reactions*, Phys. Rev. Lett. **31**, 766 (1973). DOI: 10.1103/PhysRevLett.31.766.

[2] M. Beckerman, *Sub-barrier fusion of two nuclei*, Rep. Prog. Phys. **51**, 1047 (1988). DOI: 10.1088/0034-4885/51/8/001.

[3] C. H. Dasso, S. Landowne, and A. Winther, *Channel-coupling effects in heavy-ion fusion reactions*, Nucl. Phys. A **405**, 381 (1983). DOI: 10.1016/0375-9474(83)90578-X.

[4] P. H. Stelson, *Neutron flow between nuclei as the principal enhancement mechanism in heavy-ion subbarrier fusion*, Phys. Lett. B **205**, 190 (1988). DOI: 10.1016/0370-2693(88)91647-4.

[5] N. Rowley, G. R. Satchler, and P. H. Stelson, *On the "distribution of barriers" interpretation of heavy-ion fusion*, Phys. Lett. B **254**, 25 (1991). DOI: 10.1016/0370-2693(91)90389-8.

[6] J. R. Leigh et al., *Barrier distributions from the fusion of oxygen ions with* $^{144,148,154}\mathrm{Sm}$ *and* $^{186}\mathrm{W}$, Phys. Rev. C **52**, 3151 (1995). DOI: 10.1103/PhysRevC.52.3151.

[7] A. B. Balantekin and N. Takigawa, *Quantum tunneling in nuclear fusion*, Rev. Mod. Phys. **70**, 77 (1998). DOI: 10.1103/RevModPhys.70.77.

[8] K. Hagino and N. Takigawa, *Subbarrier fusion reactions and many-particle quantum tunneling*, Prog.

Theor. Phys. **128**, 1061 (2012). DOI: 10.1143/PTP.128.1061.
[9] B. B. Back, H. Esbensen, C. L. Jiang, and K. E. Rehm, *Recent developments in heavy-ion fusion reactions*, Rev. Mod. Phys. **86**, 317 (2014). DOI: 10.1103/RevModPhys.86.317.
[10] R. G. Stokstad, Y. Eisen, S. Kaplanis, D. Pelte, U. Smilansky, and I. Tserruya, *Fusion of* $^{16}\mathrm{O} + {}^{148,150,152,154}\mathrm{Sm}$ *at sub-barrier energies*, Phys. Rev. C **21**, 2427 (1980). DOI: 10.1103/PhysRevC.21.2427.
[11] M. Dasgupta, D. J. Hinde, N. Rowley, and A. M. Stefanini, *Measuring barriers to fusion*, Annu. Rev. Nucl. Part. Sci. **48**, 401 (1998). DOI: 10.1146/annurev.nucl.48.1.401.
[12] K. Hagino, N. Rowley, and A. T. Kruppa, *A program for coupled-channel calculations with all order couplings for heavy-ion fusion reactions*, Comput. Phys. Commun. **123**, 143 (1999). DOI: 10.1016/S0010-4655(99)00243-X.
[13] J. X. Wei, J. R. Leigh, D. J. Hinde, et al., *Experimental determination of fusion-barrier distributions*, Phys. Rev. Lett. **67**, 3368 (1991). DOI: 10.1103/PhysRevLett.67.3368.
[14] H. Timmers, J. R. Leigh, M. Dasgupta, et al., *Probing fusion barrier distributions with quasi-elastic scattering*, Nucl. Phys. A **633**, 421 (1998). DOI: 10.1016/S0375-9474(98)00121-3.
[15] D. L. Hill and J. A. Wheeler, *Nuclear constitution and the interpretation of fission phenomena*, Phys. Rev. **89**, 1102 (1953). DOI: 10.1103/PhysRev.89.1102.
[16] R. A. Broglia and Å. Winther, *Heavy Ion Reactions* (Addison-Wesley, Redwood City, 1991).
[17] G. R. Satchler, *Direct Nuclear Reactions* (Clarendon Press, Oxford, 1983).
[18] H. Esbensen, *Coupled-channels analysis of fusion of* $^{16}\mathrm{O} + {}^{208}\mathrm{Pb}$, Phys. Rev. C **72**, 054607 (2005). DOI: 10.1103/PhysRevC.72.054607.
[19] L. F. Canto, P. R. S. Gomes, R. Donangelo, and M. S. Hussein, *Fusion and breakup of weakly bound nuclei*, Phys. Rep. **424**, 1 (2006). DOI: 10.1016/j.physrep.2005.10.006.
[20] C. Simenel, *Nuclear quantum many-body dynamics*, Eur. Phys. J. A **48**, 152 (2012). DOI: 10.1140/epja/i2012-12152-0.
[21] G. Montagnoli and A. M. Stefanini, *Recent experimental results in sub- and near-barrier heavy-ion fusion reactions*, Eur. Phys. J. A **53**, 169 (2017). DOI: 10.1140/epja/i2017-12350-2.
[22] C. L. Jiang, B. B. Back, H. Esbensen, K. E. Rehm, et al., *Hindrance of heavy-ion fusion at extreme sub-barrier energies*, Phys. Rev. Lett. **89**, 052701 (2002). DOI: 10.1103/PhysRevLett.89.052701.
[23] J. O. Newton, R. D. Butt, M. Dasgupta, D. J. Hinde, et al., *Systematic failure of the Woods–Saxon nuclear potential to describe near-barrier fusion*, Phys. Rev. C **70**, 024605 (2004). DOI: 10.1103/PhysRevC.70.024605.
[24] A. M. Stefanini, F. Scarlassara, S. Beghini, G. Montagnoli, et al., *Fusion of* $^{40}\mathrm{Ca} + {}^{90,96}\mathrm{Zr}$ *below and above the Coulomb barrier*, Phys. Rev. C **73**, 034606 (2006). DOI: 10.1103/PhysRevC.73.034606.
[25] R. Lindsay and N. Rowley, *The effect of nuclear surface vibrations on heavy-ion fusion*, J. Phys. G **10**, 805 (1984).
[26] K. Hagino, N. Rowley, and J. M. Yao, *Recent developments in heavy-ion fusion reactions around the Coulomb barrier*, EPJ Web Conf. **122**, 07002 (2016). DOI: 10.1051/epjconf/201612207002.
[27] S. Raman, C. W. Nestor, Jr., and P. Tikkanen, *Transition probability from the ground to the first-excited 2+ state of even–even nuclides*, At. Data Nucl. Data Tables **78**, 1 (2001). DOI: 10.1006/adnd.2001.0858.
[28] T. Kibédi and R. H. Spear, *Reduced electric-octupole transition probabilities, B(E3) — an update*, At. Data Nucl. Data Tables **80**, 35 (2002). DOI: 10.1006/adnd.2001.0871.